Mon. Not. R. Astron. Soc. **357,** 1077–1087 (2005) doi:10.1111/j.1365-2966.2005.08730.x

Extinction curves expected in young galaxies

Hiroyuki Hirashita,[1,2]★†‡ Takaya Nozawa,[3] Takashi Kozasa,[3] Takako T. Ishii[4]† and Tsutomu T. Takeuchi[5]§

[1]*Graduate School of Science, Nagoya University, Nagoya 464-8602, Japan*
[2]*SISSA/International School for Advanced Studies, Via Beirut 4, 34014 Trieste, Italy*
[3]*Division of Earth and Planetary Sciences, Graduate School of Science, Hokkaido University, Sapporo 060-0810, Japan*
[4]*Kwasan Observatory, Kyoto University, Yamashina-ku, Kyoto 607-8471, Japan*
[5]*Laboratoire d'Astrophysique de Marseille, Traverse du Siphon BP 8, 13376 Marseille Cedex 12, France*

Accepted 2004 December 10. Received 2004 December 6; in original form 2004 September 9

ABSTRACT

We investigate the extinction curves of young galaxies in which dust is supplied from Type II supernovae (SNe II) and/or pair instability supernovae (PISNe). We adopt Nozawa et al. (2003) for compositions and size distribution of grains formed in SNe II and PISNe. We find that the extinction curve is quite sensitive to internal metal mixing in supernovae (SNe). The extinction curves predicted from the mixed SNe are dominated by SiO_2 and are characterized by a steep rise from infrared to ultraviolet (UV). The dust from unmixed SNe shows a shallower extinction curve, because of the contribution from large-sized ($\sim$0.1 μm) Si grains. However, the progenitor mass is important in unmixed SNe II: if the progenitor mass is smaller than $\sim$20 $M_\odot$, the extinction curve is flat in UV; otherwise, the extinction curve rises towards the short wavelength. The extinction curve observed in a high-redshift quasar ($z = 6.2$) favours the dust production by unmixed SNe II. We also provide some useful observational quantities, so that our model might be compared with future high-z extinction curves.

Key words: supernovae: general – dust, extinction – galaxies: evolution – galaxies: high-redshift – galaxies: ISM – quasars: individual: SDSS J104845.05+463718.3.

1 INTRODUCTION

Dust grains play a crucial role in the formation and evolution of galaxies. Dust grains absorb stellar light and re-emit it in far-infrared (FIR), controlling the energy balance in the interstellar medium (ISM) and protostellar gas clouds. Also, the surface of dust grains is a site for an efficient formation of H_2 molecules (e.g. Cazaux & Tielens 2002, 2004), which act as an effective coolant in metal-poor ISM. Those effects of dust turn on even in a very metal-poor environment ($\sim$1 per cent of the solar metallicity; Hirashita & Ferrara 2002; Morgan & Edmunds 2003) and it is argued that the star formation rate is enhanced because of the first dust enrichment in the history of galaxy evolution. The first source of dust in the Universe is Type II supernovae (SNe II) or pair instability supernovae (PISNe), because the lifetime of their progenitors is short ($\sim 10^6$ yr). In the local Universe, dust grains are also produced by evolved low-mass stars (Gehrz 1989), but this production mechanism requires much longer ($\gtrsim$1 Gyr) time-scales. The first dust supplied by SNe II or PISNe may trigger the formation of low-mass stars (Schneider et al. 2003).

Because dust is important even in the early stage of galaxy evolution, it is crucial to know how much dust and what species of dust form. Todini & Ferrara (2001), following the method by Kozasa, Hasegawa & Nomoto (1989, 1991), show that dust mass produced by an Type II supernova (SN II) is roughly 0.1–0.4 $M_\odot$. They also find that SNe II form amorphous carbon with size around 300 Å and silicate grains around 10–20 Å. Schneider, Ferrara & Salvaterra (2004) extend the progenitor mass range to the regime of PISNe (140–260 $M_\odot$) and find that 30–60 $M_\odot$ of dust forms per PISN. The grain radii are distributed from 0.001 to 0.3 μm, depending on the species. The motivation for considering PISNe comes from some evidence indicating that the stars formed from metal-free gas, i.e. Population III (PopIII) stars, are very massive with a characteristic mass of a few hundred solar masses (Bromm & Larson 2004 and references therein). Such massive stars are considered to begin pair creation of electron and positron after the helium burning phase, and finally end their lives with an explosive nuclear reaction disrupting the whole star (Fryer, Woosley & Heger 2001). This explosion is called PISN.

Nozawa et al. (2003) also calculate the dust mass in the ejecta of PopIII SNe II and PISNe, carefully treating the radial density

★Postdoctoral Fellow of the Japan Society for the Promotion of Science (JSPS).
†Present address: SISSA/International School of Advanced Studies via Beirut, 4, 34014 Trieste, Italy.
‡E-mail: hirasita@sissa.it
§Postdoctoral Fellow of the JSPS for Research Abroad.

Table 1. Summary of grain species.

Species	Condition[a]	Ref[b]	Density (δ_j) (g cm^{-3})
C	u	1	2.28
Si	u	2	2.34
SiO_2	m/u	3	2.66
Fe	u	4	7.95
FeS	u	5	4.87
Fe_3O_4	m	6	5.25
Al_2O_3	m/u	7	4.01
MgO	u	8	3.59
$MgSiO_3$	m/u	9	3.20
Mg_2SiO_4	m/u	10	3.23

[a]The classifications m, u and m/u mean that the species is formed in mixed, unmixed and both supernovae, respectively.
[b]References for optical constants: (1) Edo (1983); (2) Edward (1985); (3) Philipp (1985); (4) Lynch & Hunter (1991); (5) Semenov et al. (2003); (6) Mukai (1989; for $\lambda < 0.14$ μm, we adopt the values at $\lambda = 0.14$ μm); (7) Toon, Pollack & Khare (1976); (8) Roessler & Huffman (1991); (9) Dorschner et al. (1995); (10) Jäger et al. (2003).

profile and the temperature evolution. Because it is still debated how efficiently the mixing of atoms within supernovae (SNe) occurs, Nozawa et al. (2003) treat two extreme cases for the mixing of elements: one is the unmixed case in which the original onion-like structure of elements is preserved and the other is the mixed case in which the elements are uniformly mixed within the helium core. After examining those two cases, they show that the formed dust species depend largely on the mixing of seed elements within SNe, because the dominant reactions change depending on the ratio of available elements (see Section 2.1 for a more detailed description). Nozawa et al. (2003) predict a larger dust mass than Todini & Ferrara (2001) for SNe II. How much and what kind of grain species form in SNe II and PISNe is still a matter of debate, partly depending on the degree of mixing within the He core and on the model of SNe employed in the calculations; see Woosley & Weaver (1995) for SNe II in Todini & Ferrara (2001), Heger & Woosley (2002) for PISNe in Schneider et al. (2004) and Umeda & Nomoto (2002) for PopIII SNe in Nozawa et al. (2003). The formed grain species in the calculation of Nozawa et al. (2003) are listed in Table 1.

Some observations have detected infrared radiation from extragalactic SNe II (e.g. Dwek et al. 1983; Kozasa et al. 1989; Moseley et al. 1989). This radiation has been interpreted to be originating from dust formed in SNe II. FIR and submillimetre (submm) observations of Galactic supernova (SN) remnants also have recently put further constraints on the dust mass formed in SNe II (Cas A, e.g. Arendt, Dwek & Moseley 1999; Dunne et al. 2003; Hines et al. 2004; Kepler, e.g. Morgan et al. 2003). Although FIR and submm observations are useful to know the dust amount, the emissivity, which reflects the composition, and the dust amount are degenerated in the observed FIR and submm luminosity. Therefore, in order to constrain the model of dust formation in SNe II, another independent information on the dust amount and composition is necessary.

Extinction curves are often used to investigate the dust properties (e.g. Mathis 1990). Recently, by using a sample of broad absorption line (BAL) quasars, Maiolino et al. (2004a) have shown that the extinction properties of the low-redshift ($z < 4$, where z is the redshift) sample is different from those of the high-z ($z > 4.9$) sample. This result is suggestive of a change in the dust production mechanism in the course of galaxy evolution. The highest-redshift BAL quasar in their sample, SDSS J104845.05+463718.3 (hereafter SDSS J1048+4637) at $z = 6.2$ shows a red spectrum at the rest-frame wavelength $\lambda < 1700$ Å. (In this paper, all the wavelengths are shown in the rest frame of observed galaxies.) However, at $\lambda > 1700$ Å, there is no indication of reddening. Then they suggest the extinction curve to be flat at $\lambda \gtrsim 1700$ Å and rising at $\lambda \lesssim 1700$ Å. Maiolino et al. (2004b) find that the extinction curve of SDSS J1048+4637 is different from that of low-z BAL quasars and is in excellent agreement with the SN II dust models by Todini & Ferrara (2001). It is interesting to extend their work to various dust formation models in Nozawa et al. (2003). The extinction curve should be different from SNe II to PISNe and from mixed SNe to unmixed SNe. Dust production in such various conditions is extensively investigated in Nozawa et al. (2003); hence, we aim at investigating the extinction curve based on their results.

In addition to Maiolino et al. (2004a), evidence for dust enrichment has been obtained at very high z (>5), where the cosmic age is less than 1 Gyr, by the recent submm and millimetre observations of distant quasars (Bertoldi et al. 2003; Priddey et al. 2003). At lower z ($\lesssim$5), direct indications of high-z dust comes from the reddening of background quasars (Fall, Pei & McMahon 1989; Zuo et al. 1997). The depletion of heavy elements in quasar absorption line systems also supports the presence of dust in distant systems (Pettini et al. 1994; Molaro, Vladilo & Centurion 1998; Levshakov et al. 2000; Vladilo 2002; Ledoux, Petitjean & Srianand 2003). There are several observations of extinction curves up to $z \sim 1$ by taking advantage of the gravitational lensing (Falco et al. 1999; Muñoz et al. 2004). Spectropolarimetric observations of two radio galaxies at $z \sim 1.4$ reveal the 2200-Å dust feature in scattered light (Solórzano-Iñarrea et al. 2004). However, most of the observations of extinction curves are limited to relatively low z, where dust is not only produced by SNe II, but also by evolved late-type stars. In the future, observational samples of extinction curves could be extended to high-z primeval galaxies, where dust is predominantly produced in SNe II and/or PISNe. This work could be applied to such future observations to reveal the size and composition of dust originating from SNe II or PISNe.

We first describe our theoretical treatment to calculate the extinction curves of dust produced by SNe II and PISNe in Section 2. We examine our results and provide some observationally convenient quantities in Section 3. We discuss our results from the observational viewpoint in Section 4 and finally give the conclusion of this paper in Section 5.

2 MODEL

Our aim is to derive the theoretical extinction curves of dust produced in SNe II and PISNe. We adopt the dust production model by Nozawa et al. (2003), who investigate various progenitor masses of SNe II and PISNe with a careful treatment of physical processes (internal mixing, temperature evolution, etc.).

2.1 Dust production in SNe II and PISNe

Nozawa et al. (2003) investigate the formation of dust grains in the ejecta of PopIII SNe (SNe II and PISNe, whose progenitors are initially metal-free). The calculation treats some details in comparison with Todini & Ferrara (2001): (i) the radiative transfer equation including the energy deposition of radioactive elements is solved to calculate the time evolution of gas temperature, which strongly affects the number density and size of newly formed grains; (ii) the radial profile of density of various metals is considered; (iii) unmixed and uniformly mixed cases within the helium core are considered.

Table 2. Models of dust production in supernovae (SNe).

Model	Progenitor mass ($M_\odot$)	Mixing	R_V	$\langle\sigma_d(V)/m_d\rangle$ (10^4 cm^2 g^{-1})	$\langle\sigma_d(0.3\ \mu m)/m_d\rangle$ (10^4 cm^2 g^{-1})
a	20	Mixed	2.4	0.98	2.8
b	20	Unmixed	3.3	2.2	4.4
c	170	Mixed	1.4	0.75	3.0
d	170	Unmixed	5.0	2.1	4.1
Galactic[a]	–	–	3.1	3.4	6.3

[a]Quantities derived from observational properties of the Galactic extinction properties (Spitzer 1978; Cardelli et al. 1989; Mathis 1990). We should note that it is not necessary to explain the Galactic properties with our models, because the origin, composition and size of dust are different.

In the unmixed case, Nozawa et al. (2003) assume that the original onion-like structure of elements is preserved. On the other hand, in the mixed case, they uniformly mix all the elements in the helium core. They also assume the complete formation of CO and SiO molecules, neglecting the destruction of those molecules: no carbon-bearing grain condenses in the region of $C/O < 1$ and no Si-bearing grain, except for oxide grains, condenses in the region of $Si/O < 1$. The formation of CO and SiO may be incomplete because of the destruction by energetic electron impact within SNe. Todini & Ferrara (2001) treat both formation and destruction of CO and SiO, finding that both are mostly destroyed. The decrease of CO leads to the formation of carbon grains, which could finally be oxidised with available oxygen. The destruction of SiO could decrease the formation of grains composed of SiO_2, $MgSiO_3$, and Mg_2SiO_4, and increase other oxidised grains and Si grains. Observationally, it is still debated if CO and SiO are efficiently destroyed or not. A detailed discussion on this issue can be found in appendix B of Nozawa et al. (2003).

In the unmixed ejecta, a variety of grain species (Si, Fe, Mg_2SiO_4, $MgSiO_3$, MgO, Al_2O_3, SiO_2, FeS and C) condense, while in the mixed ejecta, only oxide grains (SiO_2, $MgSiO_3$, Mg_2SiO_4, Al_2O_3 and Fe_3O_4) form. The species are summarized in Table 1. The difference in the formed species between mixed and unmixed cases is mainly derived by the formation of molecules. The carbon dust is not produced in their mixed case, because the carbon and oxygen are mixed and combined to form CO molecules. On the contrary, it forms in unmixed SNe, because there is a carbon-rich region at a certain radius of SNe. The formation of SiO molecules also affects the formed species: in the mixed ejecta only oxide silicate grains form, while in the unmixed ejecta non-oxide grains can form in oxygen-poor regions.

The size of the grains on the location of the formation site in the ejecta spans a range of 3 orders of magnitude, depending on the grain species. The size distribution function summed up over all the grain species is approximated by a broken power law. This size distribution is different from that of the SN II calculation of Todini & Ferrara (2001), which has a typical sizes of 300 Å for amorphous carbon and 10–20 Å for oxide grains. The difference mainly comes from the different treatment of the ejecta: Nozawa et al. (2003) consider the density and temperature structures within the helium core, while Todini & Ferrara (2001) do not. Schneider et al. (2004), based on the model of Todini & Ferrara (2001), find for PISNe a large range of dust size, depending on the species. Their result is similar to the mixed case in Nozawa et al. (2003).

We adopt the representative progenitor mass of SNe II as 20 $M_\odot$ and that of PISNe as 170 $M_\odot$. The size distribution of each grain species is almost independent of the progenitor mass, if the SN type is fixed (SN II or PISN), except for unmixed SNe II (Section 3.1). Therefore, we concentrate on only those two masses in this paper. However, the relative mass ratio among species mildly depends on the progenitor mass and we comment on it later showing the contribution of each species to the extinction curve (Section 3.1). We also investigate the mixed and unmixed cases. Therefore, we treat four cases: (a) mixed SNe II; (b) unmixed SNe II; (c) mixed PISNe; (d) unmixed PISNe; as summarized in Table 2. All the formulation and the results can be seen in Nozawa et al. (2003). In this paper, we assume the grains to be uniform and spherical.

In Fig. 1, we show the size distribution adopted in this paper, where the size distribution function $f_j(a)$ is defined so that $f_j(a)\,\mathrm{d}a$ is proportional to the number of grains in a radius interval $[a, a + \mathrm{d}a]$ (j indicates the species). The four figures correspond to the four cases in Table 2. The normalization of $f_j(a)$ is discussed in Section 3.4 and we only apply an arbitrary normalization to each figure.

2.2 Calculation of extinction curves

In order to calculate extinction curves, the optical constants for the grains are necessary. We adopt the references listed in Table 1 for the optical constants. By using those optical constants, we calculate the absorption and scattering cross-sections of homogeneous spherical grains with various sizes based on the Mie theory (Bohren & Huffman 1983). The efficiency factor of extinction, which is defined as the cross-section divided by the geometrical cross-section, is denoted as $Q_{\mathrm{ext},\,j}(\lambda, a)$. This efficiency factor is a function of the wavelength λ and the dust size a (j denotes the grain species).

The optical depth of grain j as a function of wavelength, $\tau_{\lambda,\,j}$, is calculated by weighting the cross-sections according to the size distribution as shown in Fig. 1:

$$\tau_{\lambda,\,j} = \int_0^\infty \pi a^2 Q_{\mathrm{ext},\,j}(\lambda,\ a)\, C f_j(a)\, \mathrm{d}a, \tag{1}$$

where C is the normalization constant related to the column density of dust. The determination of C is not important for the extinction curve because the extinction curve is presented in the form of A_λ/A_V (A_λ is the extinction in units of magnitude at wavelength λ and the V-band wavelength is 0.55 μm), where the constant C is canceled. The determination of C is necessary when we quantify the column density (equation 5). The extinction in units of magnitude is proportional to the optical depth as

$$A_{\lambda,\,j} = 1.086\tau_{\lambda,\,j}, \tag{2}$$

where $A_{\lambda,j}$ is the extinction of species j in units of magnitude as a function of λ and the factor 1.086 comes from $2.5\log_{10}e$. The total

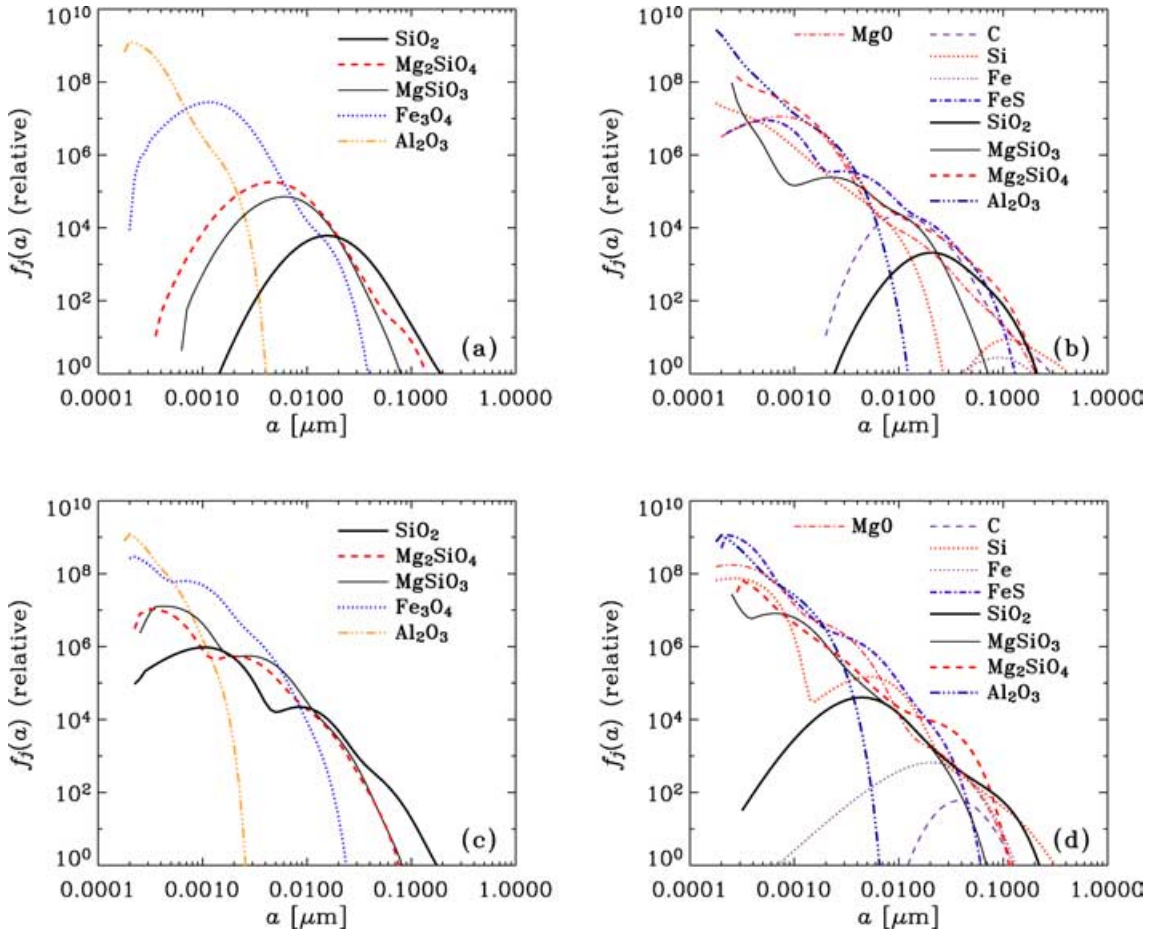

Figure 1. Size distribution function of each grain species in (a) the mixed ejecta with the progenitor of 20 $M_\odot$, (b) the unmixed ejecta with the progenitor of 20 $M_\odot$, (c) the mixed ejecta with the progenitor of 170 $M_\odot$ and (d) the unmixed ejecta with the progenitor of 170 $M_\odot$. The correspondence between the species and lines is shown in the figures.

extinction A_λ is calculated by summing $A_{\lambda,j}$ for all the concerning species:

$$A_\lambda = \sum_j A_{\lambda,j}. \tag{3}$$

3 RESULTS

3.1 Extinction curves of various SNe

In Fig. 2(a), we show the extinction curves of the four cases in Table 2: (a) mixed SNe II; (b) unmixed SNe II; (c) mixed PISNe; (d) unmixed PISNe. The contribution of each species is also shown. The extinction curve is normalized to A_V.

The extinction curves of dust produced by the mixed SNe II and PISNe are dominated by SiO_2 (Figs 2a and c). Actually, SiO_2 is the most abundant dust component in a mixed 20 $M_\odot$ SN II. However, in a 30 $M_\odot$ SN II, the production of Mg_2SiO_4 is enhanced by 2.7 times relative to that of SiO_2 and, in this case, the contribution of Mg_2SiO_4 to the extinction curve becomes 2.7 times larger. As a result, the extinction curve is dominated by the steep rising curve of Mg_2SiO_4 for $\lambda \lesssim 0.14$ μm. For the mixed 170 $M_\odot$ PISN, the extinction curve is also dominated by SiO_2. Nozawa et al. (2003) also examine a larger progenitor mass (200 $M_\odot$), where SiO_2 is the dominant species in dust mass. Therefore, we expect that the extinction curve of mixed PISNe always show a curve similar to the one in Fig. 2(c).

The extinction curve of dust produced by the unmixed SNe II (Fig. 2b) is dominated by Mg_2SiO_4 and FeS for $\lambda \lesssim 0.5$ μm. At the longer wavelength ($\lambda \gtrsim 0.5$ μm), Si dominates the curve. The extinction curves of unmixed SNe II are flatter than those of mixed SNe II, because a significant amount of large ($a \gtrsim 0.1$ μm) Si grains efficiently absorb long-wavelength photons. In a more massive SN II with the progenitor mass of 30 $M_\odot$, the production of Mg_2SiO_4 is enhanced by 2.2 times compared with Si, while the amount of FeS is almost the same; consequently the contribution of Mg_2SiO_4 to the extinction curve is enhanced by a factor of 2.2 relative to the Si contribution and the extinction curve becomes steeper. On the other hand, in less massive unmixed SNe, the production of amorphous carbon is enhanced, leading to the carbon-dominated flat extinction curve. Therefore, the extinction curve of unmixed SNe II is sensitive to the progenitor mass and the progenitor mass dependence is shown in Section 3.2.

The extinction curve of unmixed PISNe is also flat, because of Si contribution. The curve mildly rises toward ultraviolet (UV) because of contribution from Mg_2SiO_4. If the progenitor mass is 200 $M_\odot$, the production of Si is enhanced by 2 times relative to Mg_2SiO_4 and the contribution of Si becomes comparable to that of Mg_2SiO_4 even in UV. This makes the extinction curve flatter than that shown in Fig. 2(d).

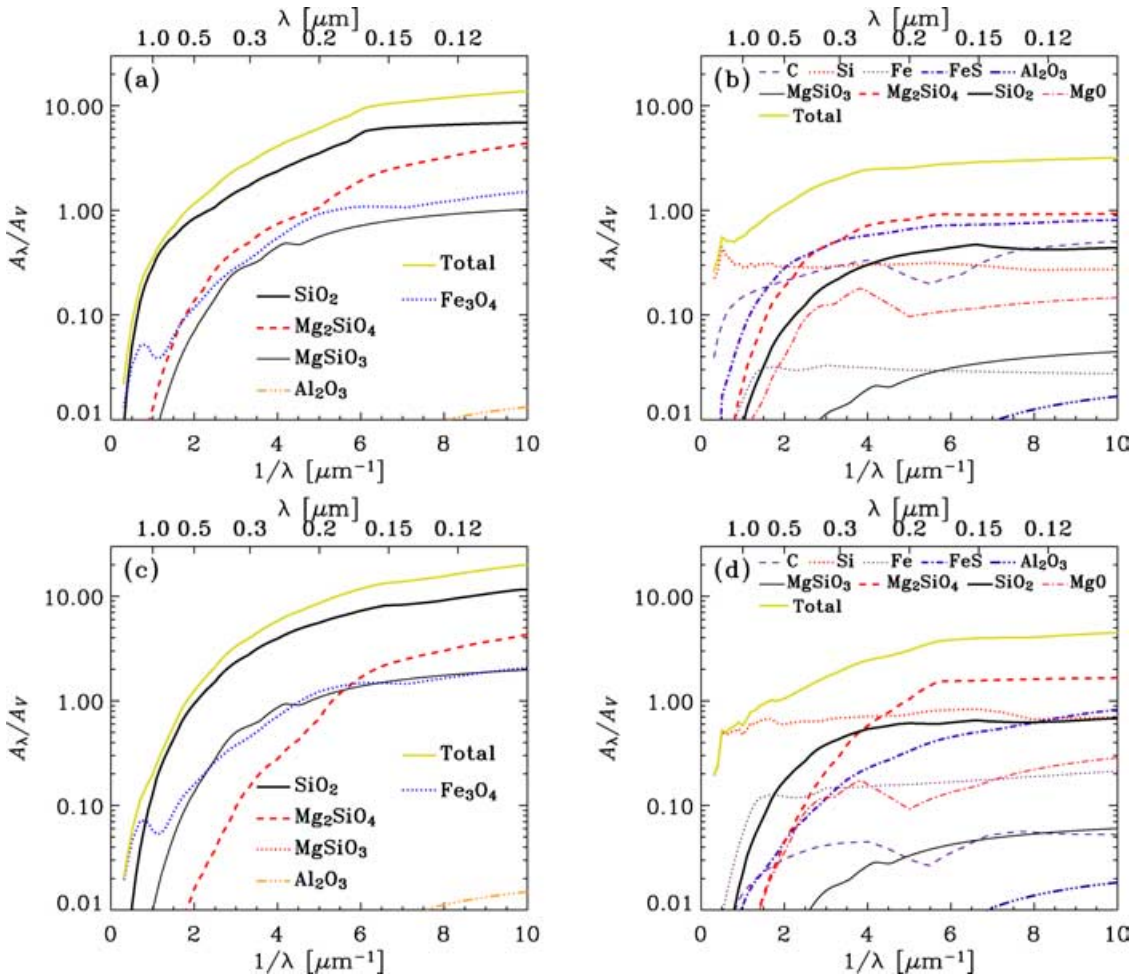

Figure 2. Extinction curves calculated for the dust production models listed in Table 2: (a) the mixed ejecta with the progenitor of 20 $M_\odot$; (b) the unmixed ejecta with the progenitor of 20 $M_\odot$; (c) the mixed ejecta with the progenitor of 170 $M_\odot$; and (d) the unmixed ejecta with the progenitor of 170 $M_\odot$. The contribution of each species is also shown. Each curve is normalized to the V-band ($\lambda = 0.55$ μm) value of the total extinction curve. The correspondence between the species and lines is shown in the figures.

In general, the extinction curves of mixed cases are steeper than those of unmixed cases. This is because the dust opacity of the mixed SNe II is dominated by small ($a \sim 0.01$ μm) SiO_2 grains. On the contrary, large Si grains produced in unmixed SNe have a large cross-section up to the near-infrared (NIR).

All the four extinction curves are compared in Fig. 3(a). We also show the extinction curves of the Galaxy (Cardelli, Clayton & Mathis 1989 with $R_V = 3.1$) and the Small Magellanic Cloud (SMC; Pei 1992). It is not necessary that our theoretical curves explain the Galactic and SMC curves because, in those two environments, dust grains are also produced by late-type stars with long lifetimes.

We do not enter deeply the infrared regime. The infrared properties of dust grains are addressed in Takeuchi et al. (in preparation; see also Takeuchi et al. 2003).

3.2 Progenitor mass dependence of unmixed SNe II

As mentioned in Section 3.1, the progenitor mass dependence is significant in the case of unmixed SNe II. Therefore, we examine various progenitor masses examined by Nozawa et al. (2003); i.e. the progenitor masses of 13, 20, 25 and 30 $M_\odot$. In Fig. 4, we present the size distribution for each species (Figs 4a, b, c and d correspond to the progenitor masses of 13, 20, 25 and 30 $M_\odot$, respectively). Based on those size distributions, we calculate the extinction curves by the method described in Section 2.2. The extinction curve as well as the contribution from each species is shown in Fig. 5. We see that the 13 $M_\odot$ extinction curve is dominated by carbon grains, whose typical size is large (∼0.1 μm). Such large carbon grains produce a flat extinction curve as presented in Fig. 5(a). As the progenitor mass becomes larger, the contribution from Si becomes larger. Although the Si extinction curve is flat, other species such as Mg_2SiO_4, FeS, Fe and SiO_2 contribute to the rising curve at short wavelengths in a complex way. As a result, if the dust production occurs in the unmixed SNe II, the extinction curve tends to be steeper as the progenitor mass becomes larger. The four extinction curves are compared in Fig. 3(b).

3.3 Comparison with standard silicate and graphite

It is useful to compare our prediction with a standard astronomical silicate in Draine & Lee (1984). Their optical constants in UV are based on olivine (Mg, Fe)$_2SiO_4$ (Huffman & Stapp 1973) and the nearest species in our model is Mg_2SiO_4. Our optical constant assumed for Mg_2SiO_4 is almost the same as that of astronomical silicate in UV, but the astronomical silicates have a larger cross-section in the optical and NIR than our Mg_2SiO_4. We calculate the extinction curve of the astronomical silicate by using the optical constant of Draine & Lee (1984) and the size distribution of Mg_2SiO_4

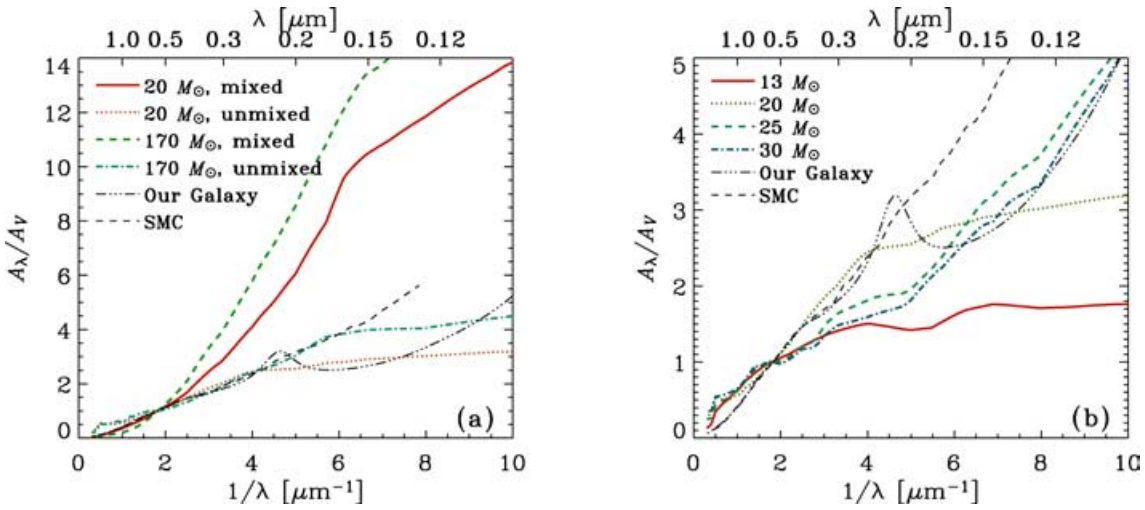

Figure 3. Comparison between the extinction curves calculated by our models. (a) Extinction curves of various types of progenitors. The thick solid, dotted, dashed and dot-dashed lines correspond to models a, b, c and d in Table 2, respectively. (b) Extinction curves for various progenitor masses of unmixed Type II supernovae (SNe II). The thick solid, dotted, dashed and dot-dashed lines correspond to the progenitor masses of 13, 20, 25 and 30 $M_\odot$, respectively. We also show the extinction curves of the Galaxy (dot-dot-dot-dashed line) and the Small Magellanic Cloud (SMC; thin dashed line) only for the reference. It is not necessary that our model explains the Galactic or SMC curve.

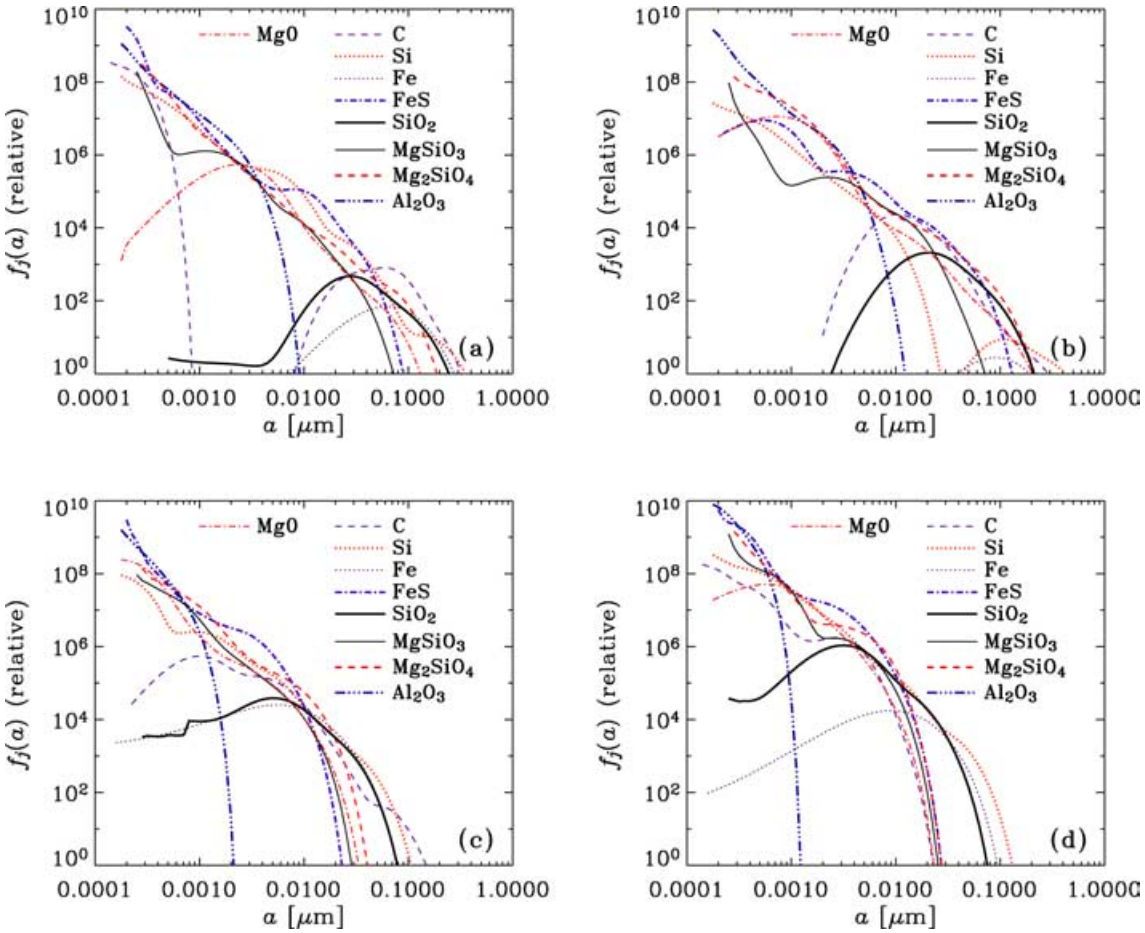

Figure 4. Size distribution function of each grain species in the unmixed ejecta with the progenitor masses of (a) 13, (b) 20, (c) 25 and (d) 30 $M_\odot$. The correspondence between the species and lines is shown in the figures.

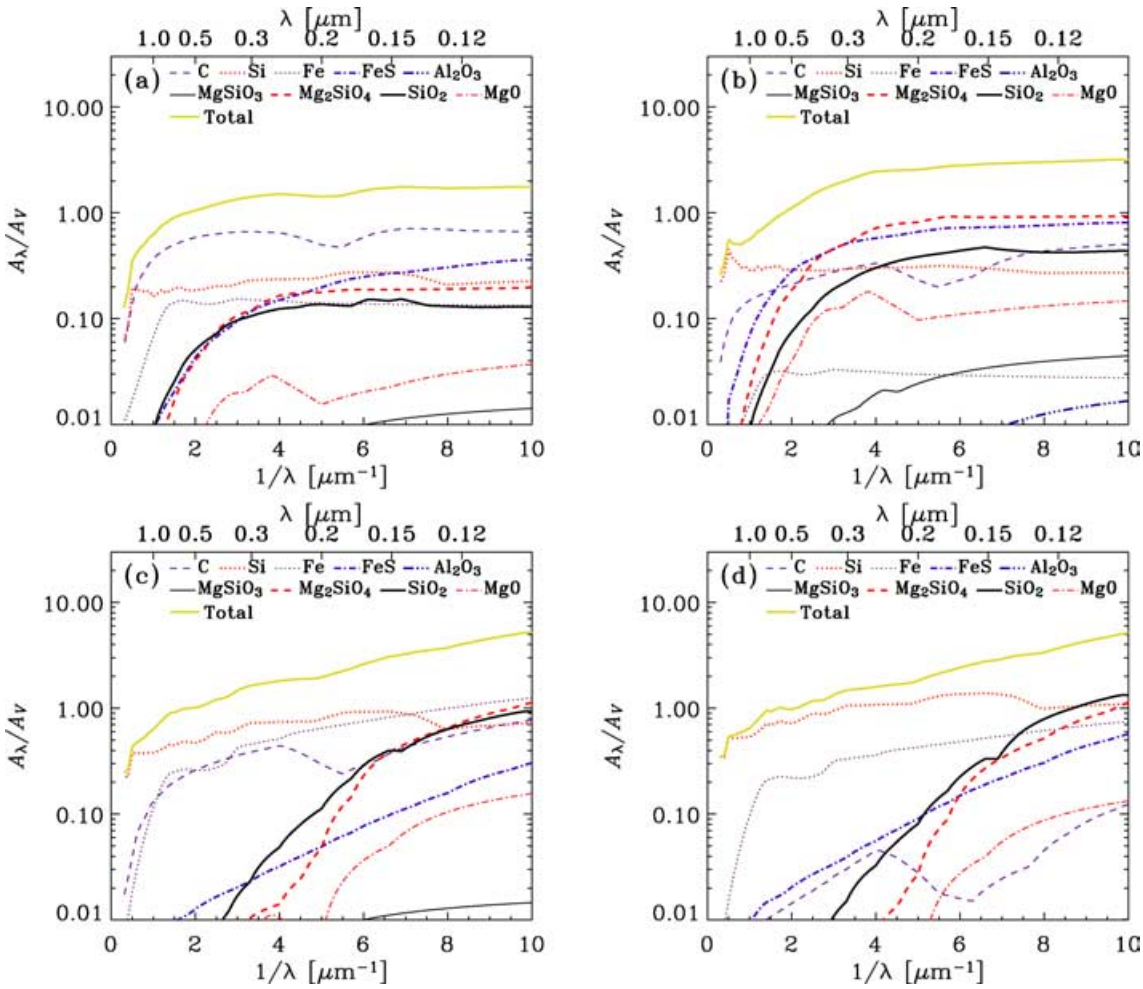

Figure 5. Extinction curves calculated for the dust production models of unmixed Type II supernova (SN II) ejecta with the progenitor masses of (a) 13, (b) 20, (c) 25 and (d) 30 $M_\odot$. Each extinction curve is normalized to the value at the V band ($\lambda = 0.55$ μm) of the total extinction curve. The contribution of each species is also shown. The correspondence between the species and lines is shown in the figures.

calculated by Nozawa et al. (2003). The extinction curve calculated by this method is the same as our extinction curve of Mg_2SiO_4 in UV but, at the V band, the difference becomes at most a factor of ∼2. Then the astronomical silicate predicts an extinction curves with a shallower slope in NIR. However, the difference does not affect our results, because the contribution of Mg_2SiO_4 is important in UV. The Mg_2SiO_4 data presented in Scott & Duley (1996) has similar optical constants to Draine & Lee (1984) in UV, and to our adopted values in optical and NIR.

The contribution of carbon grains is small in the four cases presented in Fig. 2. If we use the optical constant of graphite in Draine & Lee (1984) and the size distribution of carbon grains in Nozawa et al. (2003), we see a weak bump around 2200 Å and the overall contribution of carbon is reduced by a factor of 2. The change of carbon optical properties does not affect the total extinction. However, Nozawa et al. (2003) show that carbon becomes a principal species if the progenitor mass is around 13 $M_\odot$. In particular, the production of Mg_2SiO_4 is much reduced in a 13 $M_\odot$ SN II. Indeed, carbon grains dominate the extinction curve in 13 $M_\odot$ unmixed SNe. Regardless of which optical constant we adopt for carbon grains, we obtain a flat UV extinction curve for a 13 $M_\odot$ unmixed SN II (see Section 4.1).

3.4 Useful quantities

The extinction curve is often characterized by the parameter R_V defined as

$$R_V \equiv \frac{A_V}{E(B-V)}, \tag{4}$$

where $E(B-V) \equiv A_B - A_V$ and B indicates the B-band wavelength (0.44 μm). R_V roughly quantify the inclination of the extinction curve in the optical. The value calculated for each theoretical extinction curve is shown in Table 2.

It is also useful to relate the extinction to the dust amount, because dust mass also constrain the dust production model in galaxies (e.g. Hirashita & Ferrara 2002). For this aim, we should determine the normalization constant C in equation (1). The constant C is determined to realize the total dust column density as

$$\mu m_{\rm H} N_{\rm H} \mathcal{D} = C \sum_j \int_0^\infty \frac{4}{3}\pi a^3 \delta_j f_j(a)\,{\rm d}a\,, \tag{5}$$

where μ is the gas mass per hydrogen nucleus (assumed to be 1.4 in this paper; Spitzer 1978), $m_{\rm H}$ is the mass of a hydrogen atom, $N_{\rm H}$ is the column density of hydrogen nuclei, $\mathcal{D}$ is the dust-to-gas mass

ratio and δ_j is the material density of grain species j. We calculate δ_j from the radius per unit molecule listed in Robie & Waldbaum (1968) and the mass of atoms averaged with the isotope ratio in SN ejecta. The material density δ_j for each species is listed in Table 1.

To relate the dust cross-section to the dust mass, we define the cross-section per unit dust mass, $\langle \sigma_{\rm d}(\lambda)/m_{\rm d} \rangle$, as

$$\langle \sigma_{\rm d}(\lambda)/m_{\rm d} \rangle \equiv \frac{\sum_j \int_0^\infty \pi a^2 Q_{{\rm ext},\,j}(\lambda,\,a) f_j(a)\,{\rm d}a}{\sum_j \int_0^\infty (4/3)\pi a^3 \delta_j f_j(a)\,{\rm d}a}. \quad (6)$$

Then, the following expression of extinction is derived by using equations (1), (2), (3), (5) and (6):

$$A_\lambda = 1.086 \mu m_{\rm H} N_{\rm H} \mathcal{D} \langle \sigma_{\rm d}(\lambda)/m_{\rm d} \rangle. \quad (7)$$

We provide the values of $\langle \sigma_{\rm d}(V)/m_{\rm d} \rangle$ (the cross-section in the V band per unit dust mass) in Table 2. By using this value, the dust amount can be quantified if we know $N_{\rm H}$ from other observations (for example, observations of Lyα absorption line). Then, A_V is obtained observationally for primeval galaxies (a system in which dust is predominantly supplied by SNe II or PISNe), we obtain the dust-to-gas ratio. The colour excess $E(B-V)$ may be more easily obtained and, in this case, R_V listed in Table 2 could be used to derive the extinction A_V.

In the Galactic ISM, $N_{\rm H}/A_V = 1.9 \times 10^{21}$ cm^{-2} mag^{-1} and $\mathcal{D} = 6 \times 10^{-3}$ (Spitzer 1978). By using equation (7), we obtain $\langle \sigma_{\rm d}(V)/m_{\rm d} \rangle = 3.4 \times 10^4$ cm^2 g^{-1} for the Galactic dust. We have obtained similar values in models b and d (both assume unmixed SNe), and significantly smaller ones in models a and c (both assume mixed SNe).

The dust cross-section per mass is also calculated for a UV wavelength (0.3 μm). In Table 2, we list $\langle \sigma_{\rm d}(0.3\ \mu{\rm m})/m_{\rm d} \rangle$. The difference between the models is relatively small. Therefore, the UV dust extinction is a better tracer of the dust column density than the optical extinction.

4 OBSERVATIONAL DISCUSSION

4.1 Comparison with high-z data

At present, there are few observational works of the extinction curves at $z > 5$, where the cosmic age is shorter than 1 Gyr. With this short time-scale, the dust is predominantly formed by SNe II and PISNe, because their progenitors have short lifetimes while evolved low-mass stars require longer time-scales to evolve and produce dust. Maiolino et al. (2004b) use the extinction curve of SDSS J1048+4637 to test the hypothesis that dust is predominantly supplied by SNe II. They explain the extinction curve by the dust production model of Todini & Ferrara (2001). They also investigate various initial stellar metallicities from 0 to solar after averaging the grain properties for different SNe II over the Salpeter stellar initial mass function (IMF), and find that their theoretical extinction curves agree with the observational data of SDSS J1048+4637 in the whole metallicity range.

We also use the rest-frame UV extinction curve of SDSS J1048+4637 shown in fig. 2 of Maiolino et al. (2004b). The extinction curve is flat at $\lambda > 0.17$ μm and it increases with a smaller rate than the SMC extinction curve towards the shorter wavelength at $\lambda < 0.17$ μm. The plausible range derived by Maiolino et al. (2004b) is shown by the shaded areas in Fig. 6. In Fig. 6(a), the four theoretical curves calculated by our model are shown. The extinction curves calculated with the mixed SNe are too steep to explain the observational data.

The models with the unmixed SNe agree quite well with the observational data. The extinction curve of unmixed SNe II depends on the progenitor mass as shown in Section 3.2. In Fig. 6(b), we show the UV extinction curves of unmixed SNe II with the progenitor masses of 13, 20, 25 and 30 $M_\odot$ (solid, dotted, dashed and dot-dashed lines, respectively). The flat behaviour of the 13 $M_\odot$ extinction curve comes from the carbon contribution, which produces a slight bump around $1/\lambda \sim 4$ μm^{-1}. The rise towards the shorter wavelength is mainly caused by Mg_2SiO_4. Because the production of Mg_2SiO_4 is enhanced in the massive progenitors, the extinction curve becomes steeper for more massive progenitors. The unmixed SN II models are roughly consistent with the current observational data at high z. It is interesting to note that the observational ranges lie between the flat curve predicted for low-mass (13 and 20 $M_\odot$) progenitors and the steep curve predicted by high-mass (25 and 30 $M_\odot$) progenitors. Therefore, the mixture of unmixed SNe II with various progenitor masses may explain the observational extinction curve.

Therefore, we calculate extinction curves weighted by IMF:

$$A_\lambda(\phi) \equiv \int_{m_{\rm l}}^{m_{\rm u}} A_\lambda(m)\phi(m)\,{\rm d}m, \quad (8)$$

where m is the progenitor mass, $m_{\rm l}$ and $m_{\rm u}$ are, respectively, the lower and upper mass limits of stars that cause SNe II, $A_\lambda\,(m)$ is the extinction calculated for the progenitor mass m [correctly weighted for produced dust mass; i.e. $A_\lambda\,(m)$ is large if the progenitor produces a large amount of dust], and $\phi\,(m)$ is the IMF [the number of stars with the mass range of $[m,\, m + {\rm d}m]$ is proportional to $\phi\,(m)\,{\rm d}m$]. The normalization of $\phi\,(m)$ is not important in this paper, because the extinction curve is always shown after being normalized by A_V and the normalizing constant of $\phi\,(m)$ is cancelled out. We assume the following power-law form of the IMF:

$$\phi(m) = K m^{-(x+1)}, \quad (9)$$

where K is the normalizing constant. The Salpeter IMF is reproduced by $x = 1.35$. We examine $x = 1.35$, 0.35 and 2.35. An appropriate stellar mass range for SNe II (core collapse SNe) is selected as $m_{\rm l} = 8$ $M_\odot$ and $m_{\rm u} = 40$ $M_\odot$ (Heger & Woosley 2002). We use the calculated extinction curves of unmixed SNe II with $m = 13$, 20, 25, 30 $M_\odot$ and interpolate or extrapolate the values to obtain the extinction curves of the arbitrary progenitor mass. The slopes $x = 0.35$ (2.35) represents the case where massive (less massive) stars are selectively produced. The extinction curves weighted for the IMFs are shown in Fig. 6(c), where the thick solid, dotted and dashed lines represent the results with $x = 1.35$, 0.35 and 2.35, respectively. We also investigate the effect of varying $m_{\rm l}$ and $m_{\rm u}$ with $x = 1.35$: the thin solid and dotted lines in Fig. 6(c) show the results with $(m_{\rm l}, m_{\rm u}) = (13, 40\ M_\odot)$ and $(8,\ 30\ M_\odot)$, respectively. All the examined IMFs are summarized in Table 3, and are labeled as models A–E.

As expected from Fig. 6(b), the contribution from massive SNe II tends to increase the slope of the extinction curve. Then, models B and D predict steeper extinction curves than the data of Maiolino et al. (2004b). Therefore, the contribution from the SNe II whose progenitor mass is around 13 $M_\odot$ is necessary to obtain the flat extinction curve consistent with the observational data. However, in order to reproduce the rise towards the shorter wavelength $\lambda \lesssim 0.15$ μm, the contribution from massive SNe II is necessary. In particular, model C predicts an extinction curve slightly inconsistent around $1/\lambda \sim 8$ μm^{-1}. We should emphasize that the Salpeter IMF (model A) reproduces the observed data very well.

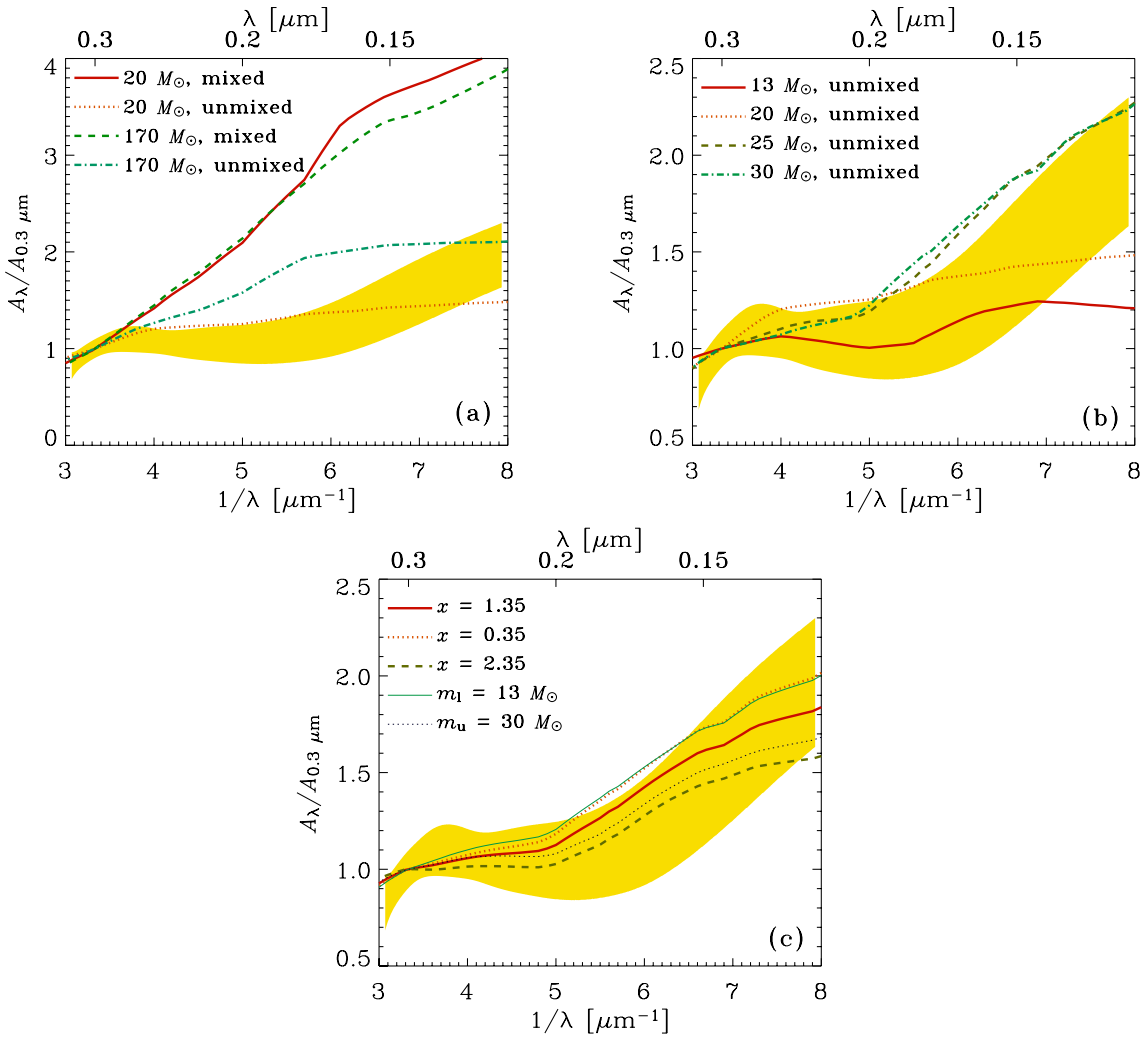

Figure 6. Ultraviolet (UV) extinction curves normalized to the extinction at 0.3 μm. The range observationally derived by Maiolino et al. (2004b) for SDSS J1048+4637 is shown by the shaded area in each figure. (a) Model predictions for various supernova (SN) models (models a–d in Table 2). (b) Results for various progenitor masses unmixed Type II supernovae (SNe II). The solid, dotted, dashed and dot-dashed lines correspond to the progenitor masses of 13, 20, 25 and 30 $M_\odot$, respectively. (c) Averaged extinction curves of unmixed SNe II. The weight of each progenitor mass is determined by initial mass functions (IMFs), which are parametrized by the power-law index (x), and the lower and upper stellar masses (m_l and m_u, respectively). The thick solid, dotted and dashed lines represent the results for $x = 1.35$, 0.35 and 2.35, respectively, with $(m_l, m_u) = (8, 40\ M_\odot)$ (models A, B, and C in Table 3, respectively). The thin solid and dotted lines show the results for $(m_l, m_u) = (13, 40\ M_\odot)$ and $(8, 30\ M_\odot)$, respectively, with $x = 1.35$ (models D and E in Table 3, respectively).

Table 3. Initial mass functions (IMFs).

Model	x	m_l ($M_\odot$)	m_u ($M_\odot$)
A	1.35	8	40
B	0.35	8	40
C	2.35	8	40
D	1.35	13	40
E	1.35	8	30

4.2 Observational strategy

A large sample of high-z quasars and galaxies will be obtained by future observations. Because the cosmic age at $z = 5$ is approximately 1 Gyr, the dust supplied by late-type stars does not dominate the total dust amount at $z > 5$. Therefore, if future observations collect a large spectroscopic sample of quasars at $z > 5$, we can directly investigate the extinction curve of dust, whose source is probably SNe II and/or PISNe. Although we have calculated the dust formation based on the PopIII progenitors, we can apply our model to metal-enriched systems as long as the dust is predominantly formed by SNe II and/or PISNe, because the dust composition and size distribution is much less sensitive to the progenitor metallicity than to the progenitor mass.

The shape of the extinction curve of high-z galaxies can be compared with the theoretical curves in this paper to constrain the size and composition of grains. The measurement of extinction enables us to measure the dust-to-gas ratio of high-z galaxies, if we use equation (7) and the cross-section per dust mass listed in Table 2. Therefore, the dust production history in high-z Universe can also be investigated based on this paper.

Some theoretical works (Bromm & Larson 2004 and references therein) suggest that first stars born from primordial gas (PopIII stars) are massive. If the gas metallicity is less than $\sim 10^{-5}\ Z_\odot$ ($Z_\odot$ is the solar metallicity), massive stars may selectively form (Schneider et al. 2003; see also Omukai 2000), causing PISNe at the end of

their lives. Therefore, the extinction curve of extremely metal-poor galaxies could be compared with our curves calculated with PISN models. The extinction curve of SDSS J1048+4637 (Maiolino et al. 2004b) has been shown to be fitted by the models of SNe II rather than those of PISNe, indicating that SDSS J1048+4637 is forming stars whose mass is $\lesssim$30 $M_\odot$. This mass range is consistent with some metallicity studies of high-z quasars (Venkatesan, Schneider & Ferrara 2004).

We finally stress that the absorption properties of dust are also important for the observation of atoms and molecules, whose detectability is affected by the dust extinction (e.g. Shibai et al. 2001). Therefore, quantifying high-z extinction is crucial to discuss the exploration of high-z Universe by atomic or molecular lines.

5 CONCLUSION

We have theoretically investigated the extinction curves of young galaxies in which dust is supplied predominantly from SNe II and/or PISNe. We have adopted Nozawa et al. (2003) for compositions and size distribution of grains formed in SNe II and PISNe. We have found that the extinction curve is quite sensitive to the internal mixing of SNe. The extinction curves of mixed SNe II and PISNe are dominated by SiO_2 and are characterized by the steep rise from NIR to UV because the main contribution comes from relatively small ($\sim$0.01 μm) grains. On the contrary, the extinction curves of dust produced in unmixed SNe II and PISNe are much flatter, because of a large contribution from large-sized $\sim$0.1 μm Si grains.

We have also derived the dust cross-section per unit dust mass. This quantity is useful to estimate the dust column density from extinction. The UV extinction traces the dust column density better than the optical extinction. The extinction also affects the observability of other molecular or atomic lines. The result of this paper can be used to estimate the extinction effect in high-z galaxies.

Finally, our results are compared with a high-z extinction curve observationally derived for SDSS J1048+4637 at $z = 6.2$ by Maiolino et al. (2004b). The comparison favours SNe II without internal mixing as sources of dust grains. The combination of various progenitor masses ranging from $\sim$10 to $\sim$30 $M_\odot$ explains well the observed extinction curve. Our theoretical extinction curves could be further utilized when a sample of high-z extinction curves is taken by future observations.

ACKNOWLEDGMENTS

We thank R. Maiolino, the referee, for useful comments, and R. Maiolino, S. Bianchi, R. Schneider and A. Ferrara for kindly providing us with their data on the extinction curve of SDSS J1048+4637. HH, TTI and TTT are supported by the Japan Society for the Promotion of Science (JSPS). TK is supported by a Grant-in-Aid for Scientific Research from JSPS (16340051). We fully utilized the NASA Astrophysics Data System (ADS) Abstract Service.

REFERENCES

Arendt R. G., Dwek E., Moseley S. H., 1999, ApJ, 521, 234
Begemann B., Dorschner J., Henning T., Mutschke H., Thamm E., 1994, ApJ, 423, L71
Bertoldi F., Carilli C. L., Cox P., Fan X., Strauss M. A., Beelen A., Omont A., Zylka R., 2003, A&A, 406, L55
Bohren C. F., Huffman D. R., 1983, Absorption and Scattering of Light by Small Particles, Wiley New York
Bromm V., Larson R. B., 2004, ARA&A, 42, 79
Cardelli J. A., Clayton G. C., Mathis J. S., 1989, ApJ, 345, 245
Cazaux S., Tielens A. G. G. M., 2002, ApJ, 575, L29
Cazaux S., Tielens A. G. G. M., 2004, ApJ, 604, 222
Dorschner J., Begemann B., Henning Th., Jaeger C., Mutschke H., 1995, A&A, 300, 503
Draine B. T., Lee H. M., 1984, ApJ, 285, 89
Dunne L., Eales S., Ivison R., Morgan H., Edmunds M., 2003, Nat, 424, 285
Dwek E. et al., 1983, ApJ, 274, 168
Edo O., 1983, PhD Thesis, Univ. Arizona
Edward D. F., 1985, in Palik E. D., ed., Handbook of Optical Constants of Solids. Academic Press, San Diego, CA, USA, p. 547
Falco E. E. et al., 1999, ApJ, 523, 617
Fall S. M., Pei Y. C., McMahon R. G., 1989, ApJ, 341, L5
Fryer C. K., Woosley S. E., Heger A., 2001, ApJ, 550, 372
Gehrz R. D., 1989, in Allamandola L. J., Tielens A. G. G. M., eds, Proc. IAU Symp. 135, Interstellar Dust. Kluwer, Dordrecht, p. 445
Heger A., Woosley S. E., 2002, ApJ, 567, 532
Hines D. C. et al., 2004, ApJS, 154, 290
Hirashita H., Ferrara A., 2002, MNRAS, 337, 921
Huffman D. R., Stapp J. L., 1973, in Greenberg J. M., van de Hulst H. C., eds, Proc. IAU Symp. 52, Interstellar Dust and Related Topics. Reidel, Dordrecht, p. 297
Jäger C., Dorschner J., Mutschke H., Posch Th., Henning Th., 2003, A&A, 408, 193
Kozasa T., Hasegawa H., Nomoto K., 1989, ApJ, 344, 325
Kozasa T., Hasegawa H., Nomoto K., 1991, A&A, 249, 474
Ledoux C., Petitjean P., Srianand R., 2003, MNRAS, 346, 209
Levshakov S. A., Molaro P., Centurión M., D'Odorico S., Bonifacio P., Vladilo G., 2000, A&A, 361, 803
Lynch D. W., Hunter W. R., 1991, in Palik E. D., ed., Handbook of Optical Constants of Solids II. Academic Press, San Diego, p. 388
Maiolino R., Oliva E., Ghinassi F., Pedani M., Mannucci F., Mujica R., Juarez Y., 2004a, A&A, 420, 889
Maiolino R., Schneider R., Oliva E., Bianchi S., Ferrara A., Mannucci F., Pedani M., Roca Sogorb M., 2004b, Nat, 431, 533
Mathis J. S., 1990, ARA&A, 28, 37
Molaro P., Vladilo G., Centurion M., 1998, MNRAS, 293, L37
Morgan H. L., Edmunds M. G., 2003, MNRAS, 343, 427
Morgan H. L., Dunne L., Eales S. A., Ivison R. J., Edmunds M. G., 2003, ApJ, 597, L33
Moseley S. H., Dwek E., Glaccum W., Graham J. R., Loewenstein R. F., 1989, Nat, 340, 697
Mukai T., 1989, in Bonetti A., Greenberg J. M., Aiello S., eds, Evolution of Interstellar Dust and Related Topics. Elsevier Science Publishers, Amsterdam, p. 397
Muñoz J., A., Falco E. E., Kochanek C. S., McLeod B. A., Mediavilla E., 2004, ApJ, 605, 614
Nozawa T., Kozasa T., Umeda H., Maeda K., Nomoto K., 2003, ApJ, 598, 785
Omukai K., 2000, ApJ, 534, 809
Pei Y. C., 1992, ApJ, 395, 130
Pettini M. H., Smith L. J., Hunstead R. W., King D. L., 1994, ApJ, 426, 79
Philipp H. R., 1985, in Palik E. D., ed., Handbook of Optical Constants of Solids. Academic Press, San Diego, p. 719
Priddey R. S., Isaak K. G., McMahon R. G., Robson E. I., Pearson C. P., 2003, MNRAS, 344, L74
Robie R. A., Waldbaum D. R., 1968, Thermodynamics Properties of Minerals and Related Substances at 298.15 Degrees K and One Atmosphere Pressure and at High Temperature, USGS Bulletin No. 1259. US Geological Survey, Reston, VA, USA
Roessler D. M., Huffman D. R., 1991, in Palik E. D., ed., Handbook of Optical Constants of Solids II. Academic Press, San Diego, CA, USA, p. 919
Schneider R., Ferrara A., Salvaterra R., Omukai K., Bromm V., 2003, Nat, 422, 869
Schneider R., Ferrara A., Salvaterra R., 2004, MNRAS, 351, 1379

Scott A., Duley W. W., 1996, ApJS, 105, 401
Semenov D., Henning Th., Helling Ch., Ilgner M., Sedlmayr E., 2003, A&A, 410, 611
Shibai H., Takeuchi T. T., Rengarajan T. N., Hirashita H., 2001, PASJ, 53, 589
Solórzano-Iñarrea C., Best P. N., Rottgering H. J. A., Cimatti A., 2004, MNRAS, 351, 997
Spitzer L. Jr, 1978, Physical Processes in the Interstellar Medium. Wiley, New York
Takeuchi T. T., Hirashita H., Ishii T. T., Hunt L. K., Ferrara A., 2003, MNRAS, 343, 839
Todini P., Ferrara A., 2001, MNRAS, 325, 726
Toon O. B., Pollack J. B., Khare B. N., 1976, J. Geophys. Res., 81, 5733
Umeda H., Nomoto K., 2002, ApJ, 565, 385
Venkatesan A., Schneider R., Ferrara A., 2004, MNRAS, 349, L43
Vladilo G., 2002, A&A, 391, 407
Woosley S. E., Weaver T. A., 1995, ApJS, 101, 181
Zuo L., Beaver E. A., Burbidge E. M., Cohen R. D., Junkkarinen V. T., Lyons R. W., 1997, ApJ, 477, 568

This paper has been typeset from a TEX/LATEX file prepared by the author.